



Quench dynamics of mass-imbalanced three-body fermionic systems in a spherical trap

A. D. Kerin  and A. M. Martin 

School of Physics, University of Melbourne, Parkville, VIC 3010, Australia



(Received 25 July 2022; accepted 2 November 2022; published 14 November 2022)

We consider a system of two identical fermions of general mass interacting with a third distinguishable particle via a contact interaction within an isotropic three-dimensional harmonic trap. We calculate time-dependent observables of the system after it is quenched in s -wave scattering length. To do this we use exact closed-form mass-imbalanced hyperspherical solutions to the static three-body problem. These exact solutions enable us to calculate two time-dependent observables, the Ramsey signal and particle separation, after the system undergoes a quench from noninteracting to the unitary regime or vice versa.

DOI: [10.1103/PhysRevA.106.053310](https://doi.org/10.1103/PhysRevA.106.053310)

I. INTRODUCTION

Investigating the dynamics of nonequilibrium quantum systems is relevant to many areas in condensed matter physics. Areas of interest include the study of superfluid turbulence, topological states, mesoscopic circuits, and can even be extended to neutron star dynamics. In these systems there are many interacting entities, making exact calculations problematic. However, it is possible to theoretically and experimentally examine quantum dynamics when there are only a few quantum bodies in the system of interest. An idealized example of such a system, where few-body quantum dynamics can be studied, is harmonically trapped quantum gases, which can be constructed at the single- to few-atom limit [1–5]. In this paper we focus on the interaction quench dynamics of three fermionic atoms trapped in a spherically symmetric harmonic trap.

We consider a system of two identical fermions which interact via a contact interaction with a third distinguishable particle, which can have a different mass. We consider the scenario where the contact interaction, between the third particle and the two identical fermions, is quenched either from the noninteracting regime to the unitary regime or vice versa. To do this we utilize the exact solutions for the system [6–11]. These exact solutions have previously been used to elucidate the thermodynamic properties of quantum gases [5,6,12–24]. In the context of quench dynamics the results presented in this paper complement previous studies in two-dimensional [25] and one-dimensional systems [26–29].

The paper is structured as follows. In Sec. II we briefly review the stationary three-body problem of two identical fermions interacting with a third distinguishable particle in a spherically symmetric harmonic trap. In Sec. III we use the eigenstates of the system to investigate the quench dynamics. In particular, we focus on quenches from the noninteracting regime to the strongly interacting (unitary) regime, a forward quench, and vice versa, a backward or reverse quench. For these two quenches we evaluate the Ramsey signal, i.e., the overlap of the time evolving state with the initial state, and

postquench evolution of the particle separation, as defined by the hyperradius. For the Ramsey signal we find that it can be calculated semianalytically for any initial state for both quenches while for the particle separation we find that it can also be calculated semianalytically for any initial state for the forward quench but the reverse quench leads to nonphysical divergences, as is the case for two-body quench dynamics [30].

II. OVERVIEW OF THE THREE-BODY PROBLEM

Our starting point is the Hamiltonian of three noninteracting bodies in a three-dimensional spherical harmonic trap,

$$\hat{H} = \sum_{k=1}^3 \left[\frac{-\hbar^2}{2m_k} \nabla_k^2 + \frac{m_k \omega^2 r_k^2}{2} \right], \quad (1)$$

where \vec{r}_k is the position of the k th particle, m_k is its mass, and ω is the trapping frequency.

In this paper we consider the case of two identical fermions interacting with a distinct third particle. We define particle one to be the impurity ($m_1 = m_i$) and particles two and three to be identical ($m = m_2 = m_3$). For convenience we define the reduced mass $\mu = m_i m / (m_i + m)$, the length scale, $a_\mu = \sqrt{\hbar / \mu \omega}$, and the mass imbalance $\kappa = m / m_i$.

For such a system the hyperspherical formulation [31] gives a closed-form solution for the wave function. However, because the interactions are enforced with the Bethe-Peierls boundary condition, the wave function can only be fully specified in the noninteracting and strongly interacting (unitary) regimes.

We define the hyperradius R and hyperangle α ,

$$R^2 = \sqrt{r^2 + \rho^2}, \quad \alpha = \arctan(r/\rho), \quad (2)$$

where

$$\vec{r} = \vec{r}_2 - \vec{r}_1, \quad (3)$$

$$\vec{\rho} = \frac{1}{\gamma} \left(\vec{r}_3 - \frac{m_i \vec{r}_1 + m \vec{r}_2}{m_i + m} \right), \quad (4)$$

$$\gamma = \frac{\sqrt{m_i(m_i + 2m)}}{m + m_i}, \quad (5)$$

and the center-of-mass (COM) coordinate is

$$\vec{C} = \frac{m_i \vec{r}_1 + m \vec{r}_2 + m \vec{r}_3}{m_i + 2m}. \quad (6)$$

The center-of-mass Hamiltonian is a simple harmonic oscillator (SHO) Hamiltonian of a single particle of mass $M = 2m + m_i$ and position \vec{C} . As such, the center-of-mass wave function is a SHO wave function. The relative Hamiltonian is given by

$$\begin{aligned} \hat{H}_{\text{rel}} = & \frac{-\hbar^2}{2\mu} \left(\frac{\partial^2}{\partial R^2} + \frac{1}{R^2 \sin(\alpha) \cos(\alpha)} \frac{\partial^2}{\partial \alpha^2} [\cos(\alpha) \sin(\alpha)] \right) \\ & + \frac{5}{R} \frac{\partial}{\partial R} - \frac{4}{R^2} - \frac{\hat{\Lambda}_r^2}{R^2 \sin(\alpha)} - \frac{\hat{\Lambda}_\rho^2}{R^2 \cos(\alpha)} \Big) + \frac{\mu\omega^2 R^2}{2}, \end{aligned} \quad (7)$$

where $\hat{\Lambda}_r^2$ and $\hat{\Lambda}_\rho^2$ are the angular momentum operators in the \hat{r} and $\hat{\rho}$ coordinate systems.

We define the trial wave function [32]

$$\psi_{3b}^{\text{rel}} = N_{qls} \frac{F_{qs}(R)}{R^2} (1 - \hat{P}_{23}) \frac{\varphi_{ls}(\alpha)}{\sin(2\alpha)} Y_{lm}(\hat{\rho}), \quad (8)$$

where N_{qls} is the normalization constant, $F_{qs}(R)$ is the hyperradial wave function, $\varphi_{ls}(\alpha) = (1 - \hat{P}_{23})\varphi_{ls}(\alpha)Y_{lm}(\hat{\rho})/\sin(2\alpha)$ is the hyperangular wave function, and \hat{P}_{23} is the particle exchange operator which swaps the positions of particles two and three.

Three conditions determine the functional forms of $F_{qs}(R)$ and $\varphi_{ls}(\alpha)$,

$$\varphi_{ls}\left(\frac{\pi}{2}\right) = 0, \quad (9)$$

$$s^2 \varphi_{ls}(\alpha) = -\varphi_{ls}''(\alpha) + \frac{l(l+1)}{\cos^2(\alpha)} \varphi_{ls}(\alpha), \quad (10)$$

$$\begin{aligned} E_{\text{rel}} = & \frac{-\hbar^2}{4\mu} \left(F''(R) + \frac{F'(R)}{R} \right) \\ & + \left(\frac{\hbar^2 s^2}{4\mu R^2} + \mu\omega^2 R^2 \right) F(R). \end{aligned} \quad (11)$$

The first is enforced because a divergence at $\alpha = \pi/2$ is non-physical, and the second and third come from the Schrödinger equation. $l \in \mathbb{Z}_{\geq 0}$ is the angular momentum quantum number, $q \in \mathbb{Z}_{\geq 0}$ and $s \in \mathbb{R}_{>0}$ are the energy eigenvalues, and the energy is given by $E_{\text{rel}} = (2q + l + s + 1)\hbar\omega$. $F_{qs}(R)$ and $\varphi_{ls}(\alpha)$ are given by [13,31,33]

$$F_{qs}(R) = \tilde{R}^s e^{-\tilde{R}^2/2} L_q^s(\tilde{R}^2), \quad (12)$$

$$\varphi_{ls}(\alpha) = \cos^{l+1}(\alpha)$$

$$\times {}_2F_1\left(\frac{l+1-s}{2}, \frac{l+1+s}{2}; l + \frac{3}{2}; \cos^2(\alpha)\right), \quad (13)$$

where $\tilde{R} = R/a_\mu$, L_q^s is a Laguerre polynomial, and ${}_2F_1$ is the Gaussian hypergeometric function.

TABLE I. Some three-body s eigenvalues at unitarity with $l = 0$ and $\kappa = 0.1, 1$, and 10 (heavy impurity, equal mass, and light impurity) to three decimal places.

$l = 0$	$\kappa = 0.1$	$\kappa = 1$	$\kappa = 10$
n	s_{nl}		
0	2.004...	2.166...	3.316...
1	5.817...	5.127...	4.707...
2	6.195...	7.114...	6.747...
3	9.685...	8.832...	8.876...

The contact interactions are enforced by the Bethe-Peierls condition [34]

$$\lim_{r_{ij} \rightarrow 0} \left[\frac{d(r_{ij}\Psi)}{dr_{ij}} \frac{1}{r_{ij}\Psi} \right] = \frac{-1}{a_s}, \quad (14)$$

where Ψ is the total three-body wave function, $r_{ij} = |\vec{r}_i - \vec{r}_j|$, and a_s is the s -wave scattering length.

In the noninteracting limit ($a_s \rightarrow 0$) Eq. (14) implies, for all values of $\kappa = m/m_i$,

$$s = \begin{cases} 2n + 4, & l = 0, \\ 2n + l + 2, & l > 0, \end{cases} \quad (15)$$

where $n \in \mathbb{Z}_{\geq 0}$. In the unitary limit ($a_s \rightarrow \infty$) the Bethe-Peierls boundary condition gives the transcendental equation

$$0 = \frac{d\varphi_{ls}}{d\alpha} \Big|_{\alpha=0} - (-1)^l \frac{(1+\kappa)^2}{\kappa\sqrt{1+2\kappa}} \varphi_{ls} \left[\arctan\left(\frac{\sqrt{1+2\kappa}}{\kappa}\right) \right]. \quad (16)$$

The values of s at unitarity for $l = 0$ and a variety of κ are given in Table I.

From this it is possible, in the noninteracting and unitary regimes, to evaluate the eigenenergies and eigenstates of the three-particle system. From this foundation, in the following section we utilize these states to evaluate the quench dynamics of this system.

III. QUENCH DYNAMICS

Below we investigate the behavior of the system after a quench in the s -wave scattering length a_s . We are interested in the forward quench (noninteracting to unitary) and the backward quench (unitary to noninteracting). Specifically, we calculate the Ramsey signal $S(t)$ and the particle separation $\langle \tilde{R}(t) \rangle$. In order to do this we need to calculate various integrals involving the wave function. First, we have the Jacobian

$$dV = d\vec{r}_1 d\vec{r}_2 d\vec{r}_3 = \frac{R^5}{4} \sin^2(2\alpha) \gamma^3 dR d\alpha d\vec{\Omega}_r d\vec{\Omega}_\rho d\vec{C}. \quad (17)$$

We make the definitions

$$\langle F_{qs}(R) | F_{qs}(R) \rangle = \int_0^\infty R F_{qs}(R)^* F_{qs}(R) dR, \quad (18)$$

$$\begin{aligned} \langle \phi_{ls}(\alpha) | \phi_{ls}(\alpha) \rangle \\ = \iiint \int_0^{\pi/2} \phi_{ls}(\alpha)^* \phi_{ls}(\alpha) 2 \sin^2(2\alpha) d\alpha d\vec{\Omega}_r d\vec{\Omega}_\rho. \end{aligned} \quad (19)$$

In this work we wish to calculate time-varying observables of a postquench system. To do this we need the time-dependent postquench wave function. The COM wave function is independent of a_s and so is unaffected by the quench. As such, we only need the time-dependent postquench *relative* wave function, which is given by

$$\begin{aligned} |\psi_{3b}^{\text{rel}}(t)\rangle &= e^{-i\hat{H}_{\text{rel}}t/\hbar} |F_{q_i s_i} \phi_{l_i s_i}\rangle \\ &= \sum_{q,s} \langle F_{qs} \phi_{l_s} | F_{q_i s_i} \phi_{l_i s_i} \rangle e^{-iE_{q_i s_i} t/\hbar} |F_{qs} \phi_{l_s}\rangle, \end{aligned} \quad (20)$$

where quantum numbers with an i subscript are the initial quantum numbers and the summation is over all eigenstates of the postquench system.

A. Ramsey signal

The Ramsey signal is defined as the wave-function overlap of the pre- and postquench wave functions, which is given by

$$\begin{aligned} S(t) &= \langle \Psi_i(t) | \Psi'(t) \rangle, \\ S(t) &= \sum_j |\langle \Psi_i(0) | \Psi'_j \rangle|^2 e^{-i(E_j - E_i)t/\hbar}, \end{aligned} \quad (21)$$

where Ψ_i is the prequench wave function with energy E_i and Ψ' is the postquench wave function. To obtain Eq. (21) we have inserted a complete set of postquench eigenstates Ψ'_j , with energies E_j , where the sum over j is a sum over all postquench eigenstates [30].

Since the COM wave function is unaffected by the quench, the Ramsey signal is given by

$$S(t) = \sum_{q,s} \left| \langle F_{q_i s_i} \phi_{l_i s_i} | F_{qs} \phi_{l_s} \rangle \right|^2 e^{-i(E_{q_i s_i} - E_{qs})t/\hbar}, \quad (22)$$

where indices with subscript i are the eigenvalues of the initial state and the unlabeled indices correspond to the postquench eigenvalues. Note that $\langle \phi_{l_s} | \phi_{l' \neq l_s} \rangle = 0$, i.e., hyperangular states of different angular momenta are orthogonal.

To evaluate the Ramsey signal we need to evaluate the hyperradial integral $\langle F_{qs} | F_{q's'} \rangle$ and the hyperangular integral $\langle \phi_{l_s} | \phi_{l's'} \rangle$.

The hyperradial integral is given by [35]

$$\begin{aligned} &\langle F_{qs}(R) | F_{q's'}(R) \rangle \\ &= \frac{a_\mu^2}{2} \binom{q+s^*}{q} \binom{q'+\frac{s'-s^*}{2}-1}{q'} \Gamma\left(\frac{s^*+s'+2}{2}\right) {}_3F_2\left(-q, \frac{s^*+s'+2}{2}, \frac{s^*-s'+2}{2}; s^*+1, \frac{s^*-s'+2}{2} - q'; 1\right). \end{aligned} \quad (23)$$

For $s = s'$ and $q \neq q'$ the hyperradial integral vanishes. Evaluating the hyperangular integral is not as straightforward as for the hyperradial integral due to the permutation operator. The hyperangle α is defined in terms of the Jacobi vectors \vec{r} and $\vec{\rho}$, which are defined in terms of \vec{r}_1 , \vec{r}_2 , and \vec{r}_3 . We have defined \vec{r} as being between particles one and two but it is possible to define \vec{r} between any pair of particles. There are then three possible ways to define the Jacobi vectors for the three-body system; these Jacobi sets are related to one another by a “kinematic rotation” [36], a coordinate transform in other words. We perform the hyperangular integral by taking advantage of these relations and “rotating” the terms acted upon by \hat{P}_{23} into the same Jacobi set as the term not acted upon by \hat{P}_{23} [37–40]. However, this restricts us to the $l = 0$ case due to the presence of the spherical harmonic term making the coordinate transform intractable for $l > 0$, as the hyperangular part of the wave function becomes a function of $\hat{\rho}$ in addition to α . For the general mass case the overlap of ϕ_{0_s} and $\phi_{0_{s'}}$ is given by

$$\begin{aligned} \langle \phi_{0_s}(\alpha) | \phi_{0_{s'}}(\alpha) \rangle &= 8\pi \int_0^{\pi/2} \left((1 - \hat{P}_{23}) \frac{\varphi_{0_s}(\alpha)}{\sin(2\alpha)} \right)^* \left((1 - \hat{P}_{23}) \frac{\varphi_{0_{s'}}(\alpha)}{\sin(2\alpha)} \right) \sin^2(2\alpha) d\alpha, \\ &= 16\pi \left[\int_0^{\pi/2} \varphi_{0_s}^*(\alpha) \varphi_{0_{s'}}(\alpha) d\alpha - \frac{(1+\kappa)^2}{2\kappa\sqrt{1+2\kappa}} \int_0^{\pi/2} \varphi_{0_s}^*(\alpha) \left[\int_{|\arctan[\sqrt{\frac{1}{\kappa}(2+\frac{1}{\kappa})}] - \alpha|}^{\pi/2 - |\pi/2 - \arctan[\sqrt{\frac{1}{\kappa}(2+\frac{1}{\kappa})}] - \alpha|} \varphi_{0_{s'}}(\alpha') d\alpha' \right] d\alpha \right]. \end{aligned} \quad (24)$$

For $l = 0$, Eq. (13) reduces to [32,38]

$$\varphi_{0_s}(\alpha) \propto \sin \left[s \left(\frac{\pi}{2} - \alpha \right) \right]. \quad (26)$$

Note that combining Eqs. (25) and (26) for $\kappa = 1$ (the equal mass case) does not give the same result as in Refs. [32,41] and only agrees when $s = s'$ is one of the solutions to Eq. (16) for $\kappa = 1$. This is because the latter references appropriately substitute Eq. (16) for $\kappa = 1$ into the result for the hyperangular integral to simplify the expression.

However, for a general value of κ we have to be more careful. For a specific κ , the s eigenvalues produced by Eq. (16)

are orthogonal to one another when Eq. (25) is evaluated only for that specific value of κ , i.e., the s eigenspectrum for $\kappa = x$ produces an orthogonal set of states only when Eq. (25) is evaluated using $\kappa = x$. However, the noninteracting values of s ($s = 4, 6, 8, \dots$) are orthogonal to one another regardless of the value of κ .

Now that we can calculate the wave-function overlaps we can evaluate the Ramsey signal for the forward and backward quenches for any initial state with $l = 0$ and any mass imbalance. In Figs. 1 and 2 we plot the forward and backward quenches, respectively, for a variety of κ and initial states.

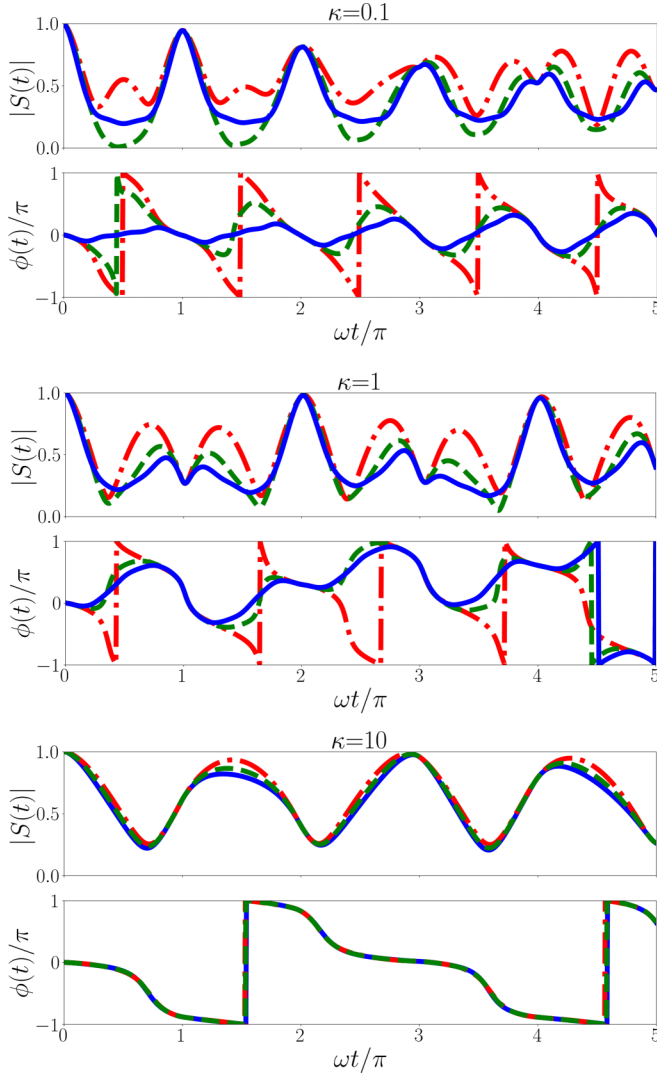


FIG. 1. Ramsey signal for the forward quench for a variety initial states and mass imbalances. In all panels, the dotted-dashed red line corresponds to $(q_i, s_i) = (0, 4)$, the dashed green line corresponds to $(q_i, s_i) = (1, 4)$, and the solid blue line corresponds to $(q_i, s_i) = (2, 4)$. The upper, middle, and lower plots correspond to $\kappa = 0.1, 1$, and 10 (heavy impurity, equal mass, and light impurity), respectively. Each Ramsey signal is obtained by evaluating Eq. (22) with ten terms in each sum, i.e., 100 terms total. In this limit we find that the sum is convergent.

Before we discuss the properties of the Ramsey signals, in Figs. 1 and 2, it is worth exploring what we may expect in a general sense. Assuming in Eq. (22) that the sum is dominated by a few terms, the general form for $S(t)$ can be represented by $S(t) \approx Ae^{-ait} + Be^{-bit} + Ce^{-cit}$. The magnitude of the signal oscillates with angular frequencies $(a - b)$, $(b - c)$, $(a - c)$ with the more heavily weighted terms being more significant. However, the *phase* of the signal is dominated by the angular frequencies of the most heavily weighted terms, not the difference between angular frequencies of different terms. In our case the angular frequencies (a, b, c, \dots) are the differences between a postquench eigenenergy and the initial energy, and the difference between the angular frequencies

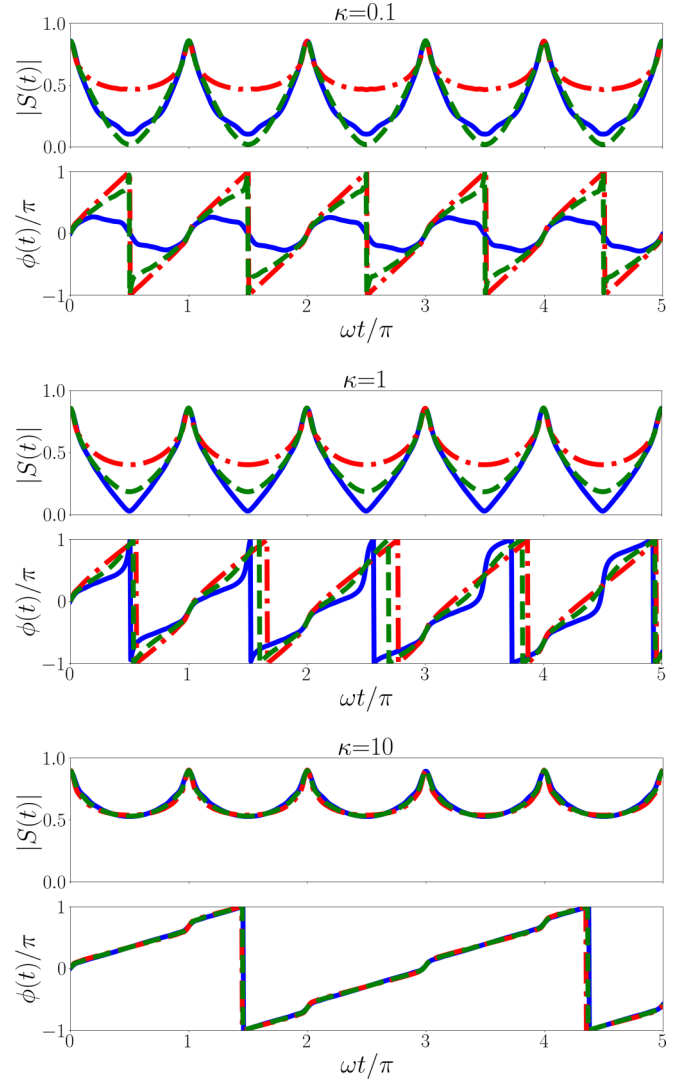


FIG. 2. Ramsey signal for the backward quench for a variety of initial states and mass imbalances. In all panels, the dotted-dashed red line corresponds to $q_i = 0$, the dashed green line corresponds to $q_i = 1$, and the solid blue line corresponds to $q_i = 2$. The upper, middle, and lower plots correspond to $\kappa = 0.1, 1$, and 10 (heavy impurity, equal mass, and light impurity) and $s_i = 2.004 \dots, 2.166 \dots$, and $3.316 \dots$, respectively. Each Ramsey signal is obtained by evaluating Eq. (22) with ten terms in each sum, i.e., 100 terms total. In this limit we find that the sum is convergent.

$[(a - b), (b - c), (a - c), \dots]$ is the difference between different postquench eigenenergies.

In Fig. 1 we plot the Ramsey signals of the forward quench for a variety of initial states and mass imbalances. We find an irregularly repeating Ramsey signal, which is in contrast to similar calculations performed for the two-body problem [30] where the signal is periodic with period π/ω . This irregular periodicity arises from the unitary s eigenspectrum. In this case angular frequencies of each term in Eq. (22) are irrational and so are the differences between them, in general. These irrational angular frequencies lead to the irregular phase and magnitude.

For the $\kappa = 0.1$ (heavy impurity) forward quench the most heavily weighted terms in Eq. (22) for the

$(q_i, s_i) = (0, 4)$ initial state (red line in the upper panel of Fig. 1) are the $|\langle F_{0,4}\phi_{0,4}|F_{0,2.004}\phi_{0,2.004}\rangle|^2 \approx 0.539$, $|\langle F_{0,4}\phi_{0,4}|F_{0,5.817}\phi_{0,5.817}\rangle|^2 \approx 0.134$, and $|\langle F_{0,4}\phi_{0,4}|F_{1,2.004}\phi_{0,2.004}\rangle|^2 \approx 0.179$ terms. The corresponding angular frequencies are $\approx -2\omega$, $\approx 1.8\omega$, and $\approx 0.004\omega$, respectively. Hence the phase displays features with a period of $\approx \pi/\omega$, and the magnitude has three main modes with periods $\approx 0.5\pi/\omega$, π/ω , and $\approx 1.1\pi/\omega$.

For the $\kappa = 1$ (equal mass) forward quench the most significant terms for the $(q_i, s_i) = (0, 4)$ initial state are $|\langle F_{0,4}\phi_{0,4}|F_{0,2.166}\phi_{0,2.166}\rangle|^2 \approx 0.499$, $|\langle F_{0,4}\phi_{0,4}|F_{0,5.127}\phi_{0,5.127}\rangle|^2 \approx 0.297$, and $|\langle F_{0,4}\phi_{0,4}|F_{1,2.166}\phi_{1,2.166}\rangle|^2 \approx 0.13$. The corresponding angular frequencies are $\approx -1.8\omega$, $\approx 1.1\omega$, and $\approx 0.17\omega$, respectively. The phase is then dominated by a mode with period $\approx 1.1\pi/\omega$ and the magnitude is dominated by modes with periods $\approx 2\pi/3\omega$, π/ω , and $\approx 2\pi/\omega$.

For the $\kappa = 10$ (light impurity) forward quench the most significant terms for the $(q_i, s_i) = (0, 4)$ initial state are $|\langle F_{0,4}\phi_{0,4}|F_{0,3.3169}\phi_{0,3.3169}\rangle|^2 \approx 0.607$, and $|\langle F_{0,4}\phi_{0,4}|F_{0,4.707}\phi_{0,4.707}\rangle|^2 \approx 0.350$. The corresponding angular frequencies are $\approx -0.7\omega/\pi$ and $\approx 0.7\omega/\pi$, respectively, hence the phase has an approximate periodicity of $2.8\pi/\omega$ and the magnitude has a period of $\approx 1.4\pi/\omega$.

In Fig. 2 we plot the Ramsey signals of the backward quench for a variety of initial states and mass imbalances. We find a strongly periodic magnitude. In the noninteracting regime we have $s = 4, 6, 8, \dots$ for every value of κ . This means that every oscillatory term in the magnitude has an angular frequency that is a multiple of two, hence the period of π/ω . However, the behavior of the phase is still dominated by the largest terms in the summation. For $\kappa = 0.1$ (heavy impurity) and $(q_i = 0, s_i = 2.0049\dots)$ the largest term is $|\langle F_{0,2.004}\phi_{0,2.004}|F_{0,4}\phi_{0,4}\rangle|^2 \approx 0.539$ and this defines the period of $\approx \pi/\omega$ we see in the phase. Similarly for $\kappa = 1$ (equal mass) and $(q_i = 0, s_i = 2.166\dots)$ the largest term is $|\langle F_{0,2.166}\phi_{0,2.166}|F_{0,4}\phi_{0,4}\rangle|^2 \approx 0.499$ defining a period of $\approx 1.1\pi/\omega$ for the phase, and for $\kappa = 10$ (light impurity) and $(q_i = 0, s_i = 3.3169\dots)$ the largest term is $|\langle F_{0,3.3169}\phi_{0,3.3169}|F_{0,4}\phi_{0,4}\rangle|^2 \approx 0.607$ defining a period of $\approx 2.8\pi/\omega$ for the phase.

B. Particle separation

The Ramsey signal is not the only quench observable we investigate. We can also calculate the expectation value of \tilde{R} , i.e., the particle separation.

The expectation value of $\tilde{R}(t)$ is given by

$$\begin{aligned}
 \langle \tilde{R}(t) \rangle &= \langle \Psi(t) | \tilde{R} | \Psi(t) \rangle \\
 &= \sum_{j, j'} \langle \Psi_i(0) | \Psi'_j \rangle \langle \Psi'_{j'} | \Psi_i(0) \rangle \langle \Psi'_j | \tilde{R} | \Psi'_{j'} \rangle e^{-i(E_j - E_{j'})t/\hbar},
 \end{aligned} \tag{27}$$

where Ψ_i is the initial prequench state with energy E_i and Ψ is the postquench state. Ψ'_j and $\Psi'_{j'}$ are eigenstates of the postquench system with eigenenergy E_j and $E_{j'}$, respectively, with the sum over j and j' taken over all postquench eigenstates.

The COM wave function is independent of the interparticle interaction and does not change when the system is quenched

and does not impact the postquench dynamics. Due to the hyperangular wave function's orthogonality in s , two sums over s and s' collapse into a single sum over s . Hence $\langle \tilde{R}(t) \rangle$ is given by

$$\begin{aligned}
 \langle \tilde{R}(t) \rangle &= \sum_{q', q} \sum_s \langle F_{q_i s_i} \phi_{l_i s_i} | F_{q' s} \phi_{l_i s} \rangle \langle F_{q s} \phi_{l_i s} | F_{q_i s_i} \phi_{l_i s_i} \rangle \\
 &\quad \times \langle F_{q' s} \phi_{l_i s} | \tilde{R} | F_{q s} \phi_{l_i s} \rangle e^{-i(E_{q' s} - E_{q s})t/\hbar}.
 \end{aligned} \tag{28}$$

All integrals required for calculating Eq. (28) are calculated in Sec. III A except for $\langle F_{q' s} | \tilde{R} | F_{q s} \rangle$. This is given by [35]

$$\begin{aligned}
 \langle F_{q s} | \tilde{R} | F_{q' s'} \rangle &= \frac{a_\mu^2}{2} \binom{q+s}{q} \binom{q'+\frac{s'}{2}-\frac{s}{2}-\frac{3}{2}}{q'} \Gamma\left(\frac{s+s'+3}{2}\right) \\
 &\quad \times {}_3F_2\left(-q, \frac{s'+s+3}{2}, \frac{s-s'+3}{2}; s+1, \right. \\
 &\quad \left. \frac{s-s'+3}{2} - q'; 1\right).
 \end{aligned} \tag{29}$$

This result, combined with the results of Sec. III A, allows us to calculate $\langle \tilde{R}(t) \rangle$ for the forward and backward quench for any initial state with $l = 0$ and any mass imbalance.

In Sec. III A we note that the magnitude and phase of the Ramsey signal for the forward quench is irregular and this is because the s eigenvalues are irrational at unitarity. Additionally, the phase for the backward quench is also irregular and this is due to the irrationality of s_i . However, the angular frequencies of the terms in Eq. (28) are always even integers because the s contributions to the energies cancel, leaving angular frequencies proportional to $(2q' - 2q)\omega$ and $q, q' \in \mathbb{Z}_{\geq 0}$. This results in the angular frequency of every term in the summation being a multiple of 2ω , causing $\langle \tilde{R}(t) \rangle$ to have a period of π/ω in both the forward and backward quench.

In Fig. 3 we have plotted $\langle \tilde{R}(t) \rangle$ for the forward quench for $\kappa = 0.1$, $\kappa = 1$, and $\kappa = 10$ (heavy impurity, equal mass, and light impurity) in the upper, middle, and lower panels, respectively. For each κ we have taken the initial state to be the ground state and calculated the sum in Eq. (28) over q, q' , and s up to $N_{\max} = 3, 6, 12$, and 24 , where N_{\max} is the number of terms in each individual sum, so there are N_{\max}^3 terms total. In each case we find that the results for $\langle \tilde{R}(t) \rangle$ have converged at $N_{\max} = 24$. As discussed above, $\langle \tilde{R}(t) \rangle$ oscillates with a period π/ω .

Additionally, we observe that as κ increases (impurity becomes lighter), the amplitude of the oscillation decreases. In the $\kappa \rightarrow \infty$ limit the unitary s eigenspectrum approaches $s \rightarrow 4, 6, 8, \dots$ [10] and the initial noninteracting ground state overlaps perfectly with the unitary ground state. As such, the amplitude decreases as κ increases until eventually $\langle \tilde{R} \rangle$ reaches a constant value of $2.18\dots$, which is $\langle \tilde{R} \rangle$ for $q = 0, s = 4$. This is also $\langle \tilde{R}(t = 0) \rangle$, so the maximum particle separation does not change with κ but the minimum increases to decrease the amplitude. Conversely, in the $\kappa \rightarrow 0$ (heavy impurity) limit, the unitary s eigenspectrum approaches $s \rightarrow 2, 6, 10, 14, \dots$, and analytically this presents a problem. The noninteracting ground state, $s_i = 4$, is orthogonal to the unitary s eigenspectrum because it is a subset

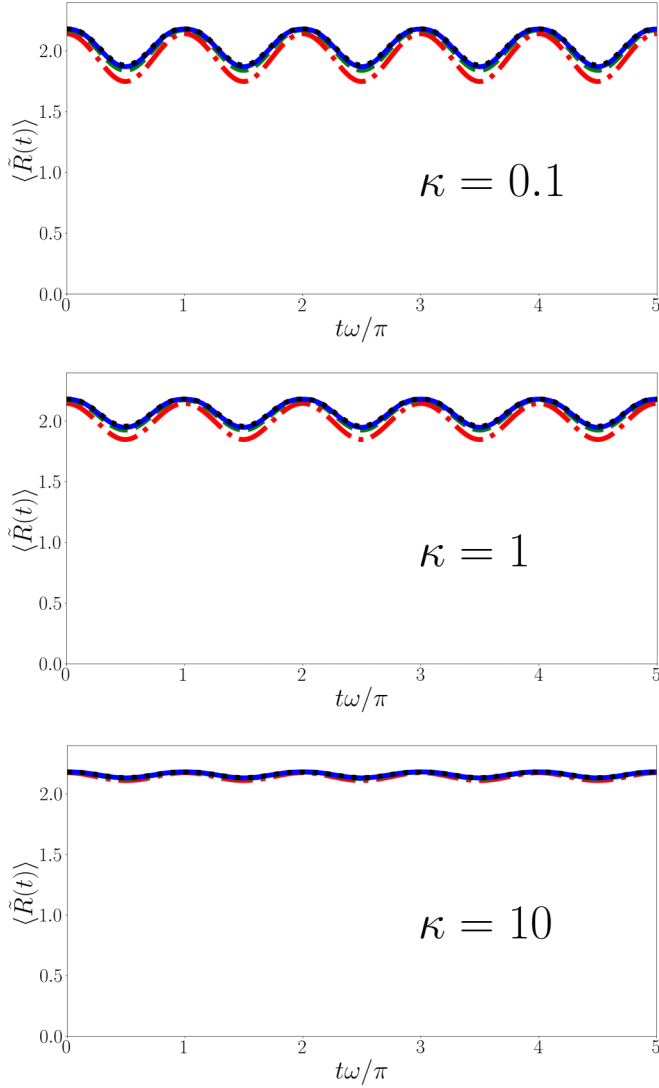


FIG. 3. $\langle \tilde{R}(t) \rangle$ for the forward quench from the noninteracting ground state, $(q_i, s_i) = (0, 4)$, for $\kappa = 0.1$ (upper panel, heavy impurity), $\kappa = 1$ (middle panel equal mass), and $\kappa = 10$ (lower panel light impurity). The dotted-dashed red line corresponds to $N_{\max} = 3$, the dashed green line to $N_{\max} = 6$, the solid blue to $N_{\max} = 12$, and the dotted black line to $N_{\max} = 24$. As can be seen from the plots, the sum is convergent with N_{\max} .

of the noninteracting eigenspectrum, except $s = 2$ which is forbidden for $l = 0$ because it causes the hyperangular part of the wave function to be zero. Numeric investigations for κ as small as 10^{-3} imply that the minimum $\langle \tilde{R}(t) \rangle$ asymptotes to $\approx 1.7 \dots$ as κ becomes very small. The maximum particle separation remains at $2.18 \dots a_\mu$ regardless of the value of κ because the initial noninteracting state does not depend on κ .

In Fig. 4 we have considered $\langle \tilde{R}(t) \rangle$ for the backward quench for the $\kappa = 0.1$, $\kappa = 1$, and $\kappa = 10$ cases (heavy impurity, equal mass, and light impurity) in the upper, middle, and lower panels, respectively. For each κ we have taken the initial state to be the ground state and calculated the sum in Eq. (28) over q , q' , and s up to $N_{\max} = 3, 6, 12$, and 24 . Similar to $r = |\vec{r}_1 - \vec{r}_2|$ in the two-body case [30] we observe in the backward quench that the particle separation diverges

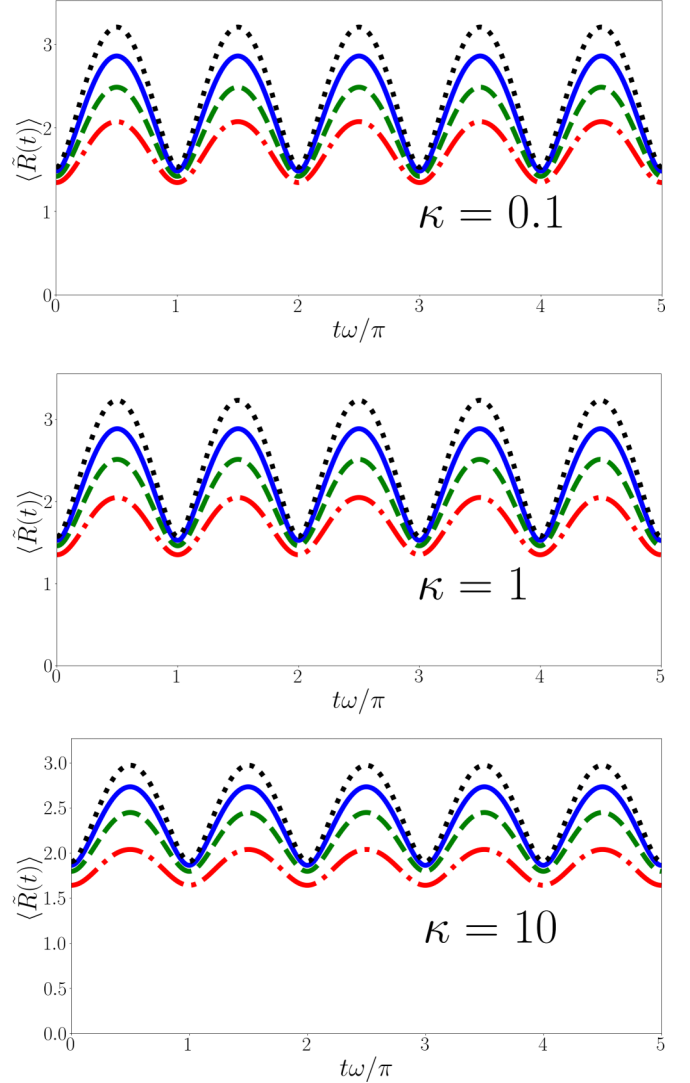


FIG. 4. $\langle \tilde{R}(t) \rangle$ for the backward quench from the interacting ground state for a variety of κ . In all panels, $q_i = 0$, in the upper panel ($\kappa = 0.1$, heavy impurity) $s_i = 2.004 \dots$, in the middle panel ($\kappa = 1$, equal mass) $s_i = 2.166 \dots$, and in the lower panel ($\kappa = 10$, light impurity) $s_i = 3.3169 \dots$. The dotted-dashed red line corresponds to $N_{\max} = 3$, the dashed green line to $N_{\max} = 6$, the solid blue to $N_{\max} = 12$, and the dotted black line to $N_{\max} = 24$. This sum diverges logarithmically with N_{\max} away from $t = n\pi/\omega$.

away from $\omega t = n\pi$. For the three-body case we find that $\langle \tilde{R}[t = (n + 1/2)\pi/\omega] \rangle$ diverges logarithmically with N_{\max} . More specifically, we find that if the number of terms in the sums over q and q' is fixed, then as more terms are included in the sum over s , $\langle \tilde{R}(t) \rangle$ converges. The divergence in $\langle \tilde{R}(t) \rangle$ comes from the sums over q and q' and therefore from the hyperradial wave function. This divergence warrants further scrutiny, so to this end we investigate the evolution of the probability distribution of $R(t)$,

$$P(R', t) = \langle \Psi(t) | \delta(R - R') | \Psi(t) \rangle. \quad (30)$$

In Fig. 5 we plot $P(R, t)$ at $t = 0, 0.17\pi/\omega, 0.34\pi/\omega$, and π/ω for $\kappa = 0.1, 1$, and 10 (heavy impurity, equal mass, and light impurity, respectively) as a function of R for the forward quench. We find that the peak of the probability distribution

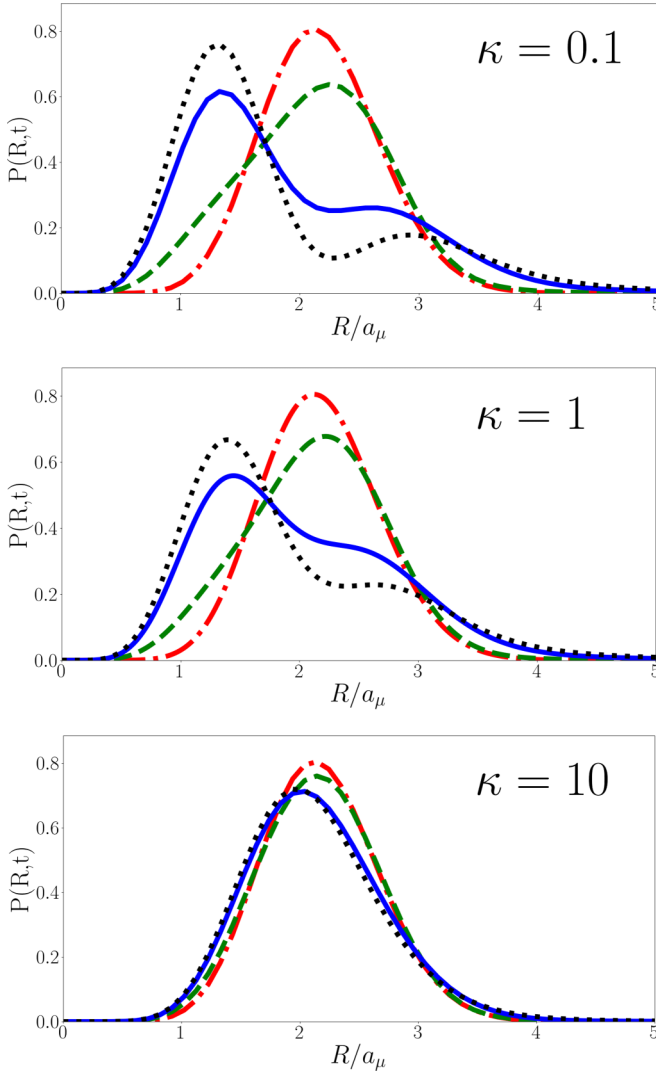


FIG. 5. The evolution of the hyperradial probability distribution, Eq. (30), following a forward quench. Each plotted curve is $P(R, t)$ for a specified value of t and the upper, middle, and lower panels correspond to $\kappa = 0.1$, 1, and 10, the heavy impurity, equal mass, and light impurity cases, respectively. The red dotted-dashed line corresponds to $t = 0$, the dashed green line to $t = 0.17\pi/\omega$, the solid blue line to $t = 0.34\pi/\omega$, and the dotted black line to $t = 0.5\pi/\omega$. For all plots the initial state is $(q_i, s_i) = (0, 4)$ and calculations are performed with $N_{\max} = 24$. Each curve is convergent with N_{\max} .

shifts inward as the system evolves, reaching its innermost point at $t = \pi/2\omega$ and then evolving in reverse back to its original configuration and continuing to oscillate in this way with period $t = \pi/\omega$. The magnitude of oscillation is smaller for larger κ . This oscillatory behavior and its dependence on κ is unsurprising given the behavior observed in Fig. 3. However, the double peak, which is present for $\kappa \lesssim 5$, is unusual. We can illuminate the double-peak structure by looking at the overlaps of the pre- and postquench wave functions. Looking at the $\kappa = 0.1$ (heavy impurity) case, the largest overlaps are $|\langle F_{0,4}\phi_{0,4}|F_{0,2.004}\phi_{0,2.004}\rangle|^2 \approx 0.539$, $|\langle F_{0,4}\phi_{0,4}|F_{0,5.817}\phi_{0,5.817}\rangle|^2 \approx 0.134$, and $|\langle F_{0,4}\phi_{0,4}|F_{1,2.004}\phi_{0,2.004}\rangle|^2 \approx 0.179$. $\langle \tilde{R} \rangle$ of these states projected onto are ≈ 1.66 , ≈ 2.56 , and

≈ 2.07 , respectively. Compare this to the $\kappa = 10$ (light impurity) case where the most significant states are $|\langle F_{0,4}\phi_{0,4}|F_{0,3.3169}\phi_{0,3.3169}\rangle|^2 \approx 0.607$, and $|\langle F_{0,4}\phi_{0,4}|F_{0,4.707}\phi_{0,4.707}\rangle|^2 \approx 0.350$ and $\langle \tilde{R} \rangle$ of the states projected onto are ≈ 2.01 and ≈ 2.33 . For small κ , the initial state most heavily overlaps with a few states, with a relatively large variation in $\langle R \rangle$ across the states. For large κ the overlaps are with a few states that are clustered in $\langle R \rangle$, hence $P(R, t = \pi/2\omega)$ is singly peaked in the latter case but doubly peaked in the former. Physically speaking, the oscillation amplitude grows smaller for a lighter impurity particle because the less mass (and therefore momenta) it has, the less it is able to affect the positions of the two fermions. For the forward quench we find $P(R, t)$ is convergent as $N_{\max} \rightarrow \infty$ at all points in time, as expected given $\langle R(t) \rangle$ is convergent for the forward quench. We now turn to the divergent case, the reverse quench.

In Fig. 6 we plot $P(R, t)$ at $t = 0, 0.17\pi/\omega, 0.34\pi/\omega$, and π/ω for $\kappa = 0.1, 1$, and 10 (heavy impurity, equal mass, and light impurity, respectively) as a function of R for the backward quench. As with the forward quench $P(R, t)$ oscillates with period π/ω , however, the peak initially moves outward rather than inward. The magnitude of the oscillations grows smaller for larger κ (lighter impurity) but the behavior is qualitatively similar regardless of the mass imbalance. For $t = n\pi/\omega$, $P(R, t)$ is approximately a Gaussian and converges with N_{\max} , however, away from $t = n\pi/\omega$ the probability distribution develops a long tail. The behavior of the tail at $t = \pi/2\omega$ for $\kappa = 1$ is plotted in Fig. 7 for various N_{\max} and the behavior is qualitatively similar for different κ . The long tail decays approximately as $1/\tilde{R}^2$ before becoming exponentially suppressed, a ‘‘cutoff.’’ The larger N_{\max} is, the later the cutoff occurs. While $P(R, t = \pi/2\omega)$ is normalized as $N_{\max} \rightarrow \infty$, this increasing long tail means that the integral of $RP(R, t = \pi/2\omega)$ from $R = 0$ to $R \rightarrow \infty$ is divergent, hence $\langle \tilde{R} \rangle$ diverges.

In the two-body case it has been suggested that the divergence in $\langle r \rangle = \langle |\vec{r}_1 - \vec{r}_2| \rangle$ is due to the $1/r$ divergence in the two-body relative wave function [30]. In the three-body case the hyperradial part of Eq. (8) does not have a $1/R$ divergence and has a cusp at $\tilde{R} \rightarrow 0$ for the unitary $\kappa = 0.1$ (heavy impurity) and $\kappa = 1$ (equal mass) ground states but not for the $\kappa = 10$ (light impurity) ground state. Nonetheless, the divergence in $\langle \tilde{R}(t) \rangle$ is present in all three cases. More specifically, we find that for $s_i < 3$ the initial wave function exhibits a cusp, while for $s_i \geq 3$ there is no cusp in the initial wave function. Regardless of which regime the initial state is in, the logarithmic divergence of $\langle \tilde{R}(t) \rangle$ persists.

However, it is clear that the finite range of the interaction in a real system provides a natural cutoff in the sum in Eq. (28). A finite range of interaction defines a minimum de Broglie wavelength which in turn defines a maximum energy which defines a maximum number of terms in the sums of Eq. (28) and thus a maximum $\langle \tilde{R}(t) \rangle$. For a system of three sodium atoms (i.e., $\kappa = 1$) in a 1-kHz trap and an interaction cutoff of 10^{-9} m we obtain a cutoff energy of $E_{\text{rel}} \approx 8.7 \times 10^6 \hbar\omega$ and thus expect a maximum $\langle \tilde{R}(t) \rangle$ of ≈ 11 . With this cutoff $\langle \tilde{R}(t) \rangle$ for the backward quench oscillates between ≈ 1.5 and ≈ 11 , with an amplitude of ≈ 5 . This is significantly larger than in the forward quench where $\langle \tilde{R}(t) \rangle$ oscillates between

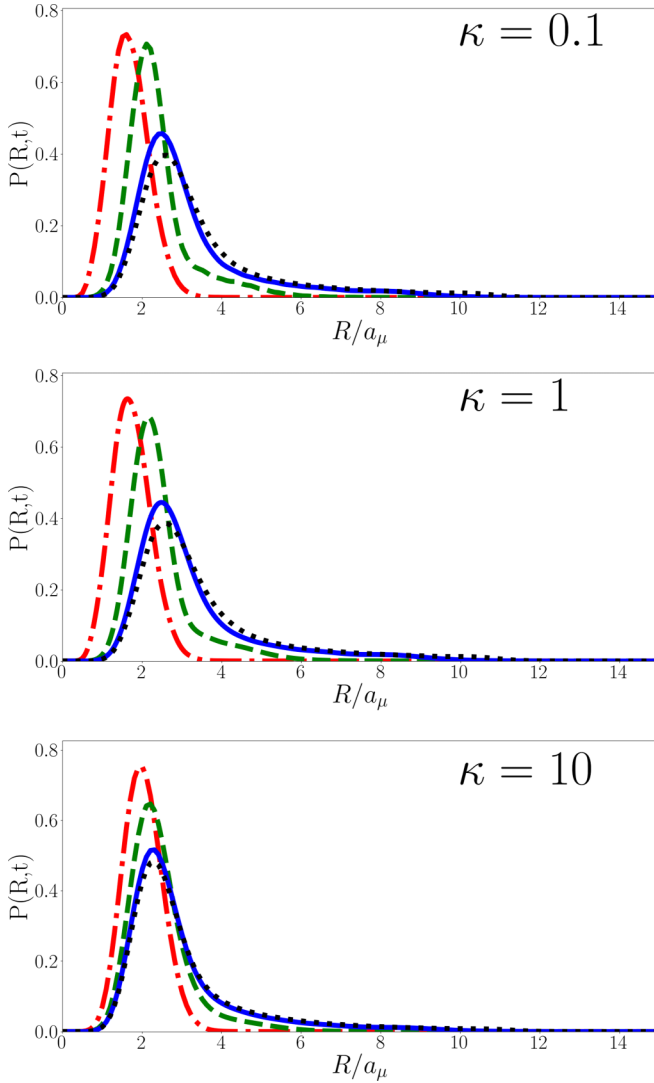


FIG. 6. The evolution of the hyperradial probability distribution, Eq. (30), following a backward quench. Each plotted curve is $P(R, t)$ for a specified value of t and the upper, middle, and lower panels correspond to $\kappa = 0.1, 1$, and 10 , the heavy impurity, equal mass, and light impurity cases, respectively. The red dotted-dashed line corresponds to $t = 0$, the dashed green line to $t = 0.17\pi/\omega$, the solid blue line to $t = 0.34\pi/\omega$, and the dotted black line to $t = 0.5\pi/\omega$. The initial state is given $q_i = 0$ for all plots, for the upper, middle, and lower plots $s_i = 2.004\dots, 2.166\dots$, and $3.3169\dots$, respectively, and all calculations are performed with $N_{\max} = 24$. Only the $t = 0$ curve (red dotted-dashed) is convergent with N_{\max} .

≈ 1.8 and ≈ 2.2 . In light of the divergence it is natural to consider the effect of using finite-range interaction models rather than zero range as done here, and the case of two bodies with a soft-core interaction has been solved analytically in a one-dimensional harmonic trap [42]. In the limit of small interaction range it is likely that the dynamics will be similar, but the effects of longer-range interactions on the dynamics are unclear. If the source of the $\langle \tilde{R}(t) \rangle$ divergence is indeed the zero-range nature of the interaction, then the finite-range model may not have the divergence present in the zero-range model.

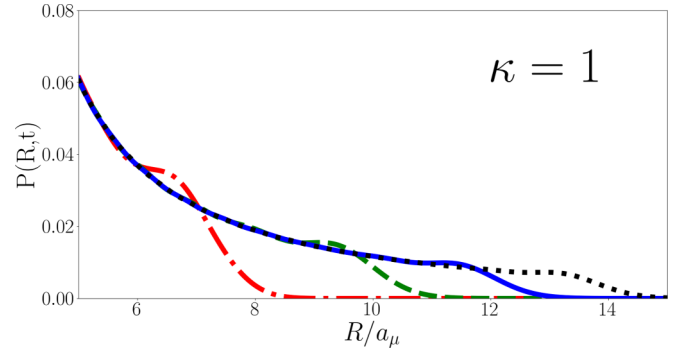


FIG. 7. The tail of $P(R, t = \pi/2\omega)$ in the reverse quench with $\kappa = 1$ (equal mass) and $(q_i, s_i) = (0, 2.166\dots)$ for various values of N_{\max} . The dotted-dashed red line corresponds to $N_{\max} = 10$, the dashed green line to $N_{\max} = 20$, the solid blue line to $N_{\max} = 30$, and the dotted black line to $N_{\max} = 40$.

However, the zero-range interaction is not the only non-physical aspect of this model. We assume that the quench in a_s is instantaneous, and in experiment a_s will change continuously over some finite time. The instantaneous quench we consider here may also be related to the $\langle \tilde{R}(t) \rangle$ divergence in the backward quench, but it is difficult to calculate a noninstantaneous quench in this formalism. In the two-body formalism it is possible to quench between any two scattering lengths [30] and thus numerically calculate a non-instantaneous quench. It would be interesting to see how this would affect the dynamics of the system and if this affects the divergence.

IV. CONCLUSION

In this paper we examine the time evolution of quenched systems. We consider a harmonically trapped system of two identical fermions plus a distinct particle interacting via a contact interaction where the system is quenched from noninteracting to strongly interacting or vice versa. We calculate the static wave function in both the noninteracting and strongly interacting regimes for general mass and use these solutions to calculate two time-dependent postquench observables: the Ramsey signal $S(t)$ and the particle separation $\langle \tilde{R}(t) \rangle$. These observables are calculated for both the forward and backward quenches.

For the Ramsey signal we find an irregularly repeating signal for the forward quench. This irregularity is due to the irrationality of the unitary energy spectrum and this irregular behavior is more pronounced for small κ (heavy impurity). For the reverse quench the magnitude of the Ramsey signal oscillates with period π/ω as the noninteracting energies are integer multiples and the phase has an irregular period due to the irrational initial energy.

For the particle separation the forward quench yields the expected oscillating result, however, the period is π/ω as the irrational contributions to the unitary eigenenergies cancel. For the backward quench we find that the particle separation diverges logarithmically, similar to divergence in $r = |\vec{r}_2 - \vec{r}_1|$ for the same quench performed on the two-body system [30]. By enforcing a cutoff based on the van der Waals interaction

range we estimate a very large amplitude of oscillation, $\approx 5a_\mu$ for $\kappa = 1$. From a physical perspective it is unclear why the divergence occurs for the backward but not forward quench but it is likely related to the zero-range interaction and/or the instantaneous quench.

Finally, we note that experimental testing of these theoretical predictions is within reach. Few-atom systems can be reliably constructed with modern techniques [1–5], the quench in s -wave scattering length can be achieved using Feshbach resonance [43–46], and the Ramsey signal can be measured using Ramsey interferometry techniques [47]. Notably, Ref. [48] measured the particle separation of two harmonically trapped ${}^6\text{Li}$ atoms following a quench in trap

geometry rather than s -wave scattering length. Additionally, there have been theoretical advances that allow for the four-body wave function to be characterized analytically in the untrapped case for $3 + 1$ and $2 + 2$ Fermi systems [49,50]. These advances may allow for this work to be generalized to the four-body case.

ACKNOWLEDGMENTS

A.D.K. is supported by an Australian Government Research Training Program Scholarship and by the University of Melbourne. We thank Victor Colussi for illuminating discussions regarding the evaluation of the hyperangular integral.

-
- [1] F. Serwane, G. Zürn, T. Lompe, T. Ottenstein, A. Wenz, and S. Jochim, *Science* **332**, 336 (2011).
- [2] S. Murmann, A. Bergschneider, V. M. Klinkhamer, G. Zürn, T. Lompe, and S. Jochim, *Phys. Rev. Lett.* **114**, 080402 (2015).
- [3] G. Zürn, A. N. Wenz, S. Murmann, A. Bergschneider, T. Lompe, and S. Jochim, *Phys. Rev. Lett.* **111**, 175302 (2013).
- [4] G. Zürn, F. Serwane, T. Lompe, A. N. Wenz, M. G. Ries, J. E. Bohn, and S. Jochim, *Phys. Rev. Lett.* **108**, 075303 (2012).
- [5] T. Stöferle, H. Moritz, K. Günter, M. Köhl, and T. Esslinger, *Phys. Rev. Lett.* **96**, 030401 (2006).
- [6] X. Cui, *Few-Body Syst.* **52**, 65 (2012).
- [7] J. P. D’Incao, J. Wang, and V. E. Colussi, *Phys. Rev. Lett.* **121**, 023401 (2018).
- [8] S. Jonsell, H. Heiselberg, and C. J. Pethick, *Phys. Rev. Lett.* **89**, 250401 (2002).
- [9] D. Blume and K. M. Daily, *Phys. Rev. Lett.* **105**, 170403 (2010).
- [10] A. Kerin and A. Martin, *arXiv:2204.09205*.
- [11] J. P. Kestner and L.-M. Duan, *Phys. Rev. A* **76**, 033611 (2007).
- [12] X.-J. Liu, H. Hu, and P. D. Drummond, *Phys. Rev. Lett.* **102**, 160401 (2009).
- [13] X.-J. Liu, H. Hu, and P. D. Drummond, *Phys. Rev. A* **82**, 023619 (2010).
- [14] D. Rakshit, K. M. Daily, and D. Blume, *Phys. Rev. A* **85**, 033634 (2012).
- [15] D. B. Kaplan and S. Sun, *Phys. Rev. Lett.* **107**, 030601 (2011).
- [16] B. C. Mulkerin, C. J. Bradly, H. M. Quiney, and A. M. Martin, *Phys. Rev. A* **85**, 053636 (2012).
- [17] B. C. Mulkerin, C. J. Bradly, H. M. Quiney, and A. M. Martin, *Phys. Rev. A* **86**, 053631 (2012).
- [18] S. Nascimbène, N. Navon, F. Jiang, K. Chevy, and C. Salomon, *Nature (London)* **463**, 1057 (2010).
- [19] M. Ku, A. Sommer, L. Cheuk, and M. Zwierlein, *Science* **335**, 563 (2012).
- [20] J. Levinsen, P. Massignan, S. Endo, and M. M. Parish, *J. Phys. B: At., Mol. Opt. Phys.* **50**, 072001 (2017).
- [21] K. M. Daily and D. Blume, *Phys. Rev. A* **81**, 053615 (2010).
- [22] V. E. Colussi, J. P. Corson, and J. P. D’Incao, *Phys. Rev. Lett.* **120**, 100401 (2018).
- [23] V. E. Colussi, B. E. van Zwol, J. P. D’Incao, and S. J. J. M. F. Kokkelmans, *Phys. Rev. A* **99**, 043604 (2019).
- [24] T. Enss, N. C. Braatz, and G. Gori, *Phys. Rev. A* **106**, 013308 (2022).
- [25] G. Bougas, S. Mistakidis, P. Giannakeas, and P. Schmelcher, *Phys. Rev. A* **106**, 043323 (2022).
- [26] D. Peřak, M. Gajda, and T. Sowiński, *New J. Phys.* **18**, 013030 (2016).
- [27] A. G. Volosniev, *Few-Body Syst.* **58**, 54 (2017).
- [28] L. M. A. Kehrberger, V. J. Bolsinger, and P. Schmelcher, *Phys. Rev. A* **97**, 013606 (2018).
- [29] T. Sowiński and M. Á. García-March, *Rep. Prog. Phys.* **82**, 104401 (2019).
- [30] A. D. Kerin and A. M. Martin, *Phys. Rev. A* **102**, 023311 (2020).
- [31] F. Werner and Y. Castin, *Phys. Rev. Lett.* **97**, 150401 (2006).
- [32] F. Werner, Ph.D. thesis University of Paris, 2008.
- [33] F. Werner and Y. Castin, *Phys. Rev. A* **74**, 053604 (2006).
- [34] H. Bethe and R. Peierls, *Proc. R. Soc. London, Ser. A* **148**, 146 (1935).
- [35] H. M. Srivastava, H. A. Mavromatis, and R. S. Alassar, *Appl. Math. Lett.* **16**, 1131 (2003).
- [36] E. Nielsen, D. V. Fedorov, A. S. Jensen, and E. Garrido, *Phys. Rep.* **347**, 373 (2001).
- [37] D. V. Fedorov and A. S. Jensen, *Phys. Rev. Lett.* **71**, 4103 (1993).
- [38] D. V. Fedorov and A. Jensen, *J. Phys. A: Math. Gen.* **34**, 6003 (2001).
- [39] E. Braaten and H.-W. Hammer, *Phys. Rep.* **428**, 259 (2006).
- [40] M. Thøgersen, *arXiv:0908.0852*.
- [41] V. E. Colussi, *Atoms* **7**, 19 (2019).
- [42] P. Kořcik and T. Sowiński, *Sci. Rep.* **8**, 48 (2018).
- [43] U. Fano, *Nuovo Cimento* **12**, 154 (1935).
- [44] H. Feshbach, *Ann. Phys.* **5**, 357 (1958).
- [45] E. Tiesinga, B. J. Verhaar, and H. T. C. Stoof, *Phys. Rev. A* **47**, 4114 (1993).
- [46] C. Chin, R. Grimm, P. Julienne, and E. Tiesinga, *Rev. Mod. Phys.* **82**, 1225 (2010).
- [47] M. Cetina, M. Jag, R. S. Lous, I. Fritsche, J. T. Walraven, R. Grimm, J. Levinsen, M. M. Parish, R. Schmidt, M. Knap *et al.*, *Science* **354**, 96 (2016).
- [48] Q. Guan, V. Klinkhamer, R. Klemt, J. H. Becher, A. Bergschneider, P. M. Preiss, S. Jochim, and D. Blume, *Phys. Rev. Lett.* **122**, 083401 (2019).
- [49] S. Endo and Y. Castin, *Phys. Rev. A* **92**, 053624 (2015).
- [50] Y. Castin, C. Mora, and L. Pricoupenko, *Phys. Rev. Lett.* **105**, 223201 (2010).